JOURNAL OF SYNCHROTRON RADIATION
ISSN 1600-5775

Solid/liquid-interface-dependent synthesis and immobilization of copper-based particles nucleated by X-ray-radiolysis-induced photochemical reaction

Akinobu Yamaguchi,[a]* Ikuya Sakurai,[b] Ikuo Okada,[b] Hirokazu Izumi,[c] Mari Ishihara,[c] Takao Fukuoka,[a] Satoru Suzuki[a] and Yuichi Utsumi[a]

[a]Laboratory of Advanced Science and Technology for Industry, University of Hyogo, 3-1-2 Kouto, Kamigori, Hyogo 678-1205, Japan, [b]Aichi Synchrotron Radiation Center, 250-3 Minamiyamaguchi-cho, Seto-shi, Aichi 489-0965, Japan, and [c]Hyogo Prefectural Institute of Technology, 3-1-12 Yukihira, Suma, Kobe 654-0037, Japan. *Correspondence e-mail: yamaguti@lasti.u-hyogo.ac.jp

Received 14 January 2020
Accepted 13 April 2020

Edited by Y. Amemiya, University of Tokyo, Japan

Keywords: X-ray radiolysis; particle nucleation; particle growth; interface.

X-ray-radiolysis-induced photochemical reaction of a liquid solution enables the direct synthesis and immobilization of nano/micro-scale particles and their aggregates onto a desired area. As is well known, the synthesis, growth and aggregation are dependent on the pH, additives and X-ray irradiation conditions. In this study, it was found that the topography and composition of synthesized particles are also dependent on the types of substrate dipped in an aqueous solution of $Cu(COOCH_3)_2$ in the X-ray-radiolysis-induced photochemical reaction. These results are attributed to the fact that a secondary electron induced by the X-ray irradiation, surface or interface on which the particles are nucleated and grown influences the particle shape and composition. This study will shed light on understanding a novel photochemical reaction route induced under X-ray irradiation. The development of this process using the X-ray-radiolysis-induced photochemical reaction in aqueous liquids enables us to achieve the rapid and easy operation of the synthesis, growth and immobilization of special nano/micro-scale complex materials or multifunctional composites.

1. Introduction

Interfaces and surfaces are of utmost importance in both physical and chemical reactions. Many studies have been carried out investigating these reactions. Here, we focus on the preparation of metal and oxide nano/microparticles on various substrates as it is a key issue in all fields of modern science and technology covering electronics, photonics, catalysis, biotechnology and so on. Electrochemical and electroless wet chemical deposition and other methods utilizing lasers (Bae *et al.*, 2002; Akamatsu *et al.*, 2004), ion beams (Yamaguchi *et al.*, 2005), electron beams (Jonah & Miller, 1977), X-rays (Ma *et al.*, 2000; Borse *et al.*, 2004; Karadas *et al.*, 2005; Oyanagi *et al.*, 2014; Yamaguchi *et al.*, 2015, 2016*a*,*b*, 2017, 2019; Saegusa *et al.*, 2019; Bharti *et al.*, 2016; Remita *et al.*, 2007) and γ-rays (Bárta *et al.*, 2010; Dey, 2005) have also been studied for incorporating metal clusters onto substrates in the desired chemical and morphological states. In particular, photochemical processes induced by broad-sense light irradiation in heterogeneous systems have been widely used in recent years because of their easy operation and wide applications. Of particular interest are photochemical reactions and processes on inorganic metal and oxide surfaces. Many excellent studies have appeared in recent years demonstrating the various possible ways with which the support materials control the

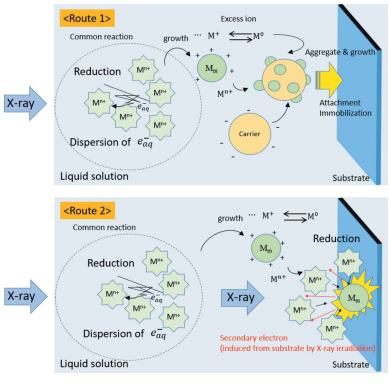

photochemical reaction properties. The reduction effect induced by the additive alcohol has also been investigated in sonochemistry, hydrothermal microwave irradiation and photochemical reactions using UV, laser, X-ray and γ-ray irradiation. The role of support materials is to assist the electron transfer resulting in reduction of metal or oxide particles and clusters, frequently having the functionality as scavenger (Yamaguchi *et al.*, 2016*b*, 2017, 2019; Saegusa *et al.*, 2019; Dey, 2005).

The synthesis of cupric particles has attracted considerable attention due to their fundamental importance and potential future applications (Siegfried & Choi, 2005; Zoolfakar *et al.*, 2014; Meyer *et al.*, 2012; Su *et al.*, 2015; Poizot *et al.*, 2000; Tamaki *et al.*, 1998; Wang *et al.*, 1996; Zaman *et al.*, 2011, 2012; Izaki *et al.*, 2007; Zhang *et al.*, 2014; Wang *et al.*, 2018; Volanti *et al.*, 2008). Cupric oxides are p-type semiconductor materials with narrow band gap energy, resulting in their use in the anodes of lithium ion cells and solar-cell panels, *etc*. Until now, using a hydrothermal microwave oven technique has enabled synthesis of CuO nanostructures (Zaman *et al.*, 2012; Zhang *et al.*, 2014; Volanti *et al.*, 2008). Recently, Wang *et al.* have succeeded in synthesizing the novel candy-like Cu_4O_3 microstructure by facile wet chemical synthesis (Wang *et al.*, 2018). They have also reported long-term antibacterial activities of the candy-like Cu_4O_3 microstructure. Caltrop cupric oxide micro/nanoparticles including both Cu_2O and CuO have been directly synthesized from $Cu(COOCH_3)_2$ aqueous solution by X-ray radiolysis with additive alcohols (Yamaguchi *et al.*, 2017, 2019; Saegusa *et al.*, 2019). Recently, it has been found that alkyl alcohols with a chain length longer than four are unable to synthesize any particles in aqueous solutions of $Cu(COOCH_3)_2$ due to X-ray-radiolysis-induced photochemical reaction (Yamaguchi *et al.*, 2019). From these results it is deduced that the solvable ratio of alcohol to water plays a significant role in the synthesis, growth and aggregation of particles. Thus, the recent investigations reveal, to some extent, the controllability of particle synthesis by the X-ray-radiolysis-induced photochemical reaction.

X-ray irradiation can provide radicals from the radiolysis of liquids and secondary electron generation from substrates dipped in liquid solution. There are two possible routes for the nucleation and immobilization of particles. One is a normal process (Route 1) which sequentially precedes nucleation, growth and aggregation in the liquid solution (La Mer & Dinegar, 1950; La Mer, 1952), schematically illustrated in Fig. 1(*a*). The grown particles are attached onto a substrate through van der Waals interactions and finally immobilized. In the other route (Route 2) particles are generated on the surface of the substrate and particles reduced by secondary electron generation from the substrate by X-ray irradiation are involved in particle growth on the substrate surface, as shown in Fig. 1(*b*). Therefore, the nucleation, growth and aggregation of particles could be influenced, in particular, near the surface of the substrate and the interface between the particles and substrate. We should investigate the controllability of cupric particle synthesis by type of substrate on which the synthesized particles are grown and immobilized in

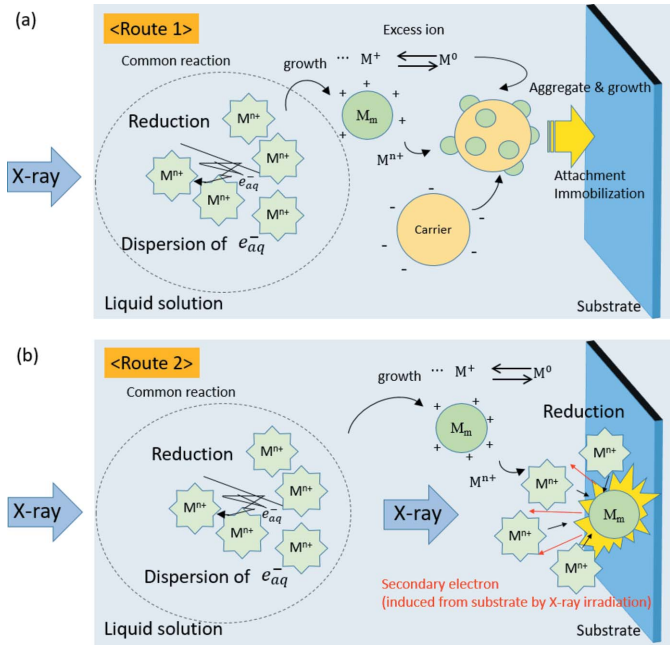

Figure 1
Schematic diagram of particles synthesized in X-ray-radiolysis-induced photochemical reaction in a liquid and near the surface of a substrate dipped in solution. (*a*) Route 1 shows the series of particle nucleation, growth, ripening and aggregation induced by the X-ray-radiolysis-induced photochemical reaction in a liquid solution. After the particle ripening is partially completed, it adheres to the surface of the substrate. (*b*) Route 2 shows that a secondary electron induced from the substrate by X-ray irradiation contributes to the reduction of metallic ions and precedes the nucleation and growth of particles on the surface of substrate.

liquid solution using X-ray-radiolysis-induced photochemical reaction to understand the mechanism of particle nucleation, ripening and aggregation. In this study, we study the substrate type dependence of synthesis, growth and immobilization of cupric particles by X-ray-induced photochemical reaction using synchrotron radiation.

2. Experiments

We performed synchrotron-radiation-induced X-ray radiolysis experiments using beamline BL8S2 at the Aichi Synchrotron Radiation Center, Aichi Science and Technology Foundation (Yamaguchi *et al.*, 2015, 2016*a*,*b*, 2017, 2019; Saegusa *et al.*, 2019). The storage ring current and energy were in operation at 300 mA and 1.2 GeV with super-bending magnets of 5 T. The X-ray spectrum is displayed in Fig. 2(*a*). The substrates except $LiNbO_3$ were purchased from the Nilaco Corporation (https://nilaco.jp/en/), a specialized trading company which mainly treats various materials for scientific researchers and engineers. The pure grade for Cu, Al and Ni plates was 99.96%, 99+% and 99%, respectively. Silicon substrates were 'eleven nines' and doped. $LiNbO_3$ substrates were purchased from Yamaju Ceramics Co. Ltd – they were purchased in the form of plates and cut into 10 mm × 10 mm pieces for use. Substrate cleaning was performed after ultrasonic cleaning

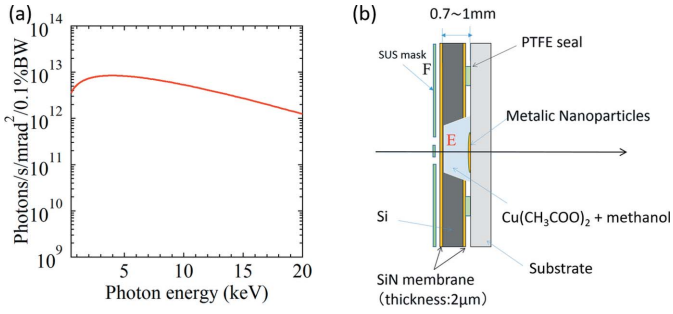

Figure 2
(*a*) X-ray spectrum for this experimental setup at BL8S1 of Aichi Synchrotron Radiation Center. (*b*) Schematic of the X-ray irradiation experimental setup. This cell, used for the X-ray radiolysis process, was insulated from the ground. All electrons participating in the reduction process are supplied from X-ray irradation only. There is no flow of electrons from the ground to the substrate/liquid interface.

with pure water and acetone. The silicon substrate was not subjected to a process for removing a naturally occurring oxide layer. Here, we prepared 20 ml aliquots of 0.05 *M* (mol L^{-1}) $Cu(COOCH_3)_2$ (purchased from FUJIFILM Wako Pure Chemical Corporation, Wako 1st Grade) as a stock solution. In this study we used an ultra-pure water prepared by a Milli-Q system (Merck KGaA). We siphoned off 200 µL of the stock solution into a microtube and added 1 µL of methanol to obtain the mixed solution. The methanol was also purchased as Wako 1st Grade from FUJIFILM Wako Pure Chemical Corporation. We siphoned off 20 µL aliquots of the mixed solution and poured it into the apparatus for the liquid irradiation. To investigate the substrate type dependence of the X-ray-radiolysis-induced photochemical reaction, each substrate listed in Table 1 (size: 10 mm × 10 mm) was dipped into the solution in the apparatus as schematically illustrated in Fig. 2(*b*). Then the specimen was exposed to polychromatic X-ray irradiation (for 5 min). The cell used for the X-ray radiolysis process was then insulated from the ground. In this experimental setup there was no flow of electrons from the ground to the substrate/liquid interface. All electrons participating in the reduction process were supplied from X-ray irradiation. After the irradiation, the specimen temperature was anticipated to be raised by about 15°C. After 5 min of X-ray irradiation some particles and their aggregates were deposited and immobilized on the substrate. The substrate was taken from the specimen and gently washed with ionized water to remove residual materials. The residual dross was adequately removed but the immobilized particles were not. The particles on each substrate were examined by field emission scanning electron microscopy (FE-SEM; Jeol JSM-7001F) with energy-dispersive X-ray spectroscopy (EDX) to perform topological and elemental analyses. We also measured the Raman spectra of the particles using a micro-Raman spectrometer (NR-5100; JASCO). The excitation source had a wavelength of 532 nm, a power of 3.2 mW and was magnified using a 100× field lens. The laser spot size was about 1 µm. All experiments were performed at room temperature and in ambient atmosphere.

Table 1
Summary of substrates dipped in the cell.

Number	Substrate
1	SiO_2/Si
2	Si(100) n-type, sheet resistivity, 1–10 Ω cm
3	Si(100) p-type, sheet resistivity, 1–20 Ω cm
4	Cu
5	Ni
6	Al
7	128° Y-cut $LiNbO_3$
8	PTFE

3. Results and discussion

Scanning electron microscope (SEM) images of particles synthesized and immobilized on the substrates listed on Table 1 by X-ray-radiolysis-induced-photochemical reaction in the solution are shown in Figs. 3–10. Comparing these figures, the particle shape and elemental composition were found to be strongly dependent on the type of substrate. For example, relatively sharp shaped particles tended to synthesize on Ni, n-doped Si(100), p-doped Si(100) and Al substrates; various shaped particles immobilized on the SiO_2/Si and Cu substrates; and distorted particles formed on the $LiNbO_3$ and polytetrafluorethylene (PTFE) substrates.

Next, to investigate the composition of the substrate dependence of cupric particles synthesized by the X-ray-radiolysis-induced photochemical reaction, the micro-Raman spectra were measured. Fig. 11 shows a summary of Raman spectra of the particles synthesized and immobilized on each substrate described in Table 1. Comparing these spectra obtained from (*a*) SiO_2/Si, (*b*) n-doped Si and (*c*) p-doped Si substrates, we notice that the obtained Raman spectra are almost the same. This result indicates that the composition of

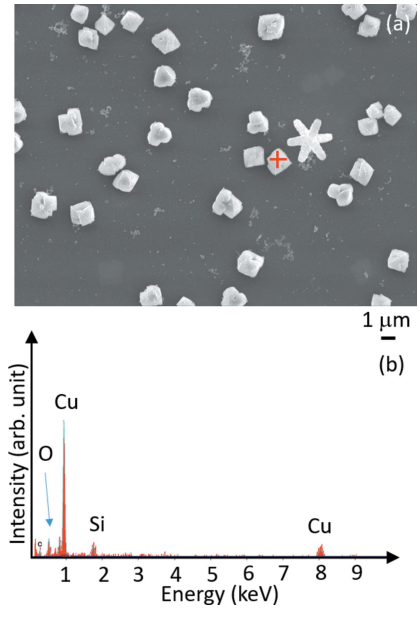

Figure 3
(*a*) SEM image of particles deposited on SiO_2/Si substrate dopped in a $Cu(COOCH_3)_2$ solution with methanol after X-ray irradiation for 5 min. (*b*) The EDX spectrum measured from the position indicated by the red cross mark in (*a*).

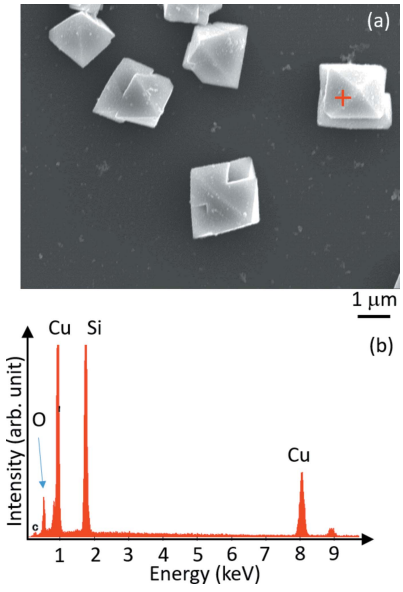

Figure 4
(*a*) SEM image and (*b*) EDX spectrum of particles synthesized and deposited on an n-doped Si substrate.

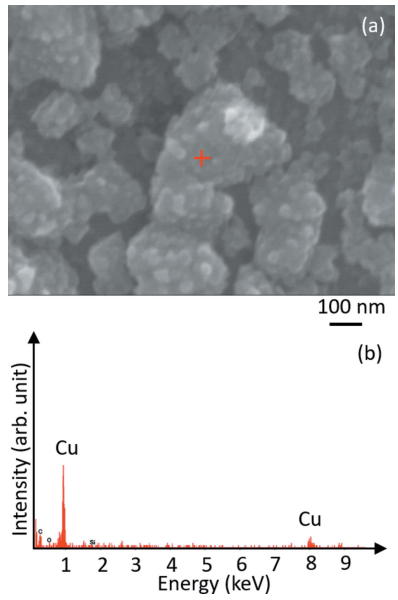

Figure 6
(*a*) SEM image and (*b*) EDX spectrum of particles synthesized and deposited on a Cu substrate.

the synthesized particles deposited on the silicon substrates is independent of doping but the morphology is strongly dependent on the surface crystalline nature. This fact is easily understandable from the viewpoint of the crystal growth mechanism.

The Raman spectrum obtained from the particles grown on the Cu substrate is quite different from those of the others. Besides, we notice that the Raman spectrum of particles on Ni, $LiNbO_3$ and PTFE substrates are also unique. The Raman spectrum of particles on Al substrates is almost the same as those Raman spectra obtained from the SiO_2/Si and Si substrates. There are three cupric oxides candidates: CuO, Cu_2O and Cu_4O_3. Peaks at 283, 333 and 622 cm^{-1} are deduced to be Raman signals from the Ag (283.8 cm^{-1}) and Bg (333.5 and 622.5 cm^{-1}) modes of cupric oxide CuO. Here, according to Debbichi *et al.* (2012), the Ag and Bg peaks denote the Raman modes only with the oxygen atom displacement along the *b* direction and perpendicular to the *b* axis, respectively. The Raman spectra from particles on SiO_2, n-doped Si, p-doped Si and Al substrates are expected to be almost origi-

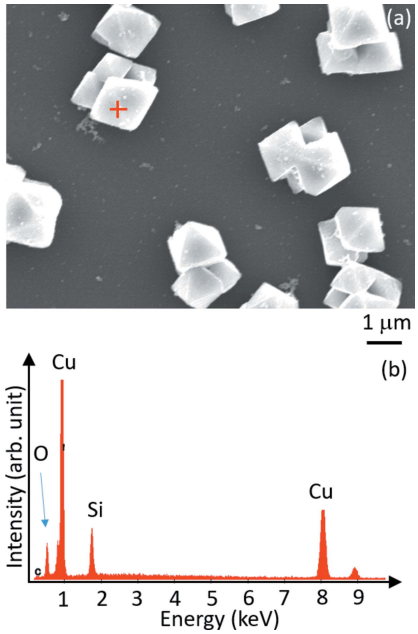

Figure 5
(*a*) SEM image and (*b*) EDX spectrum of particles synthesized and deposited on a p-doped Si substrate.

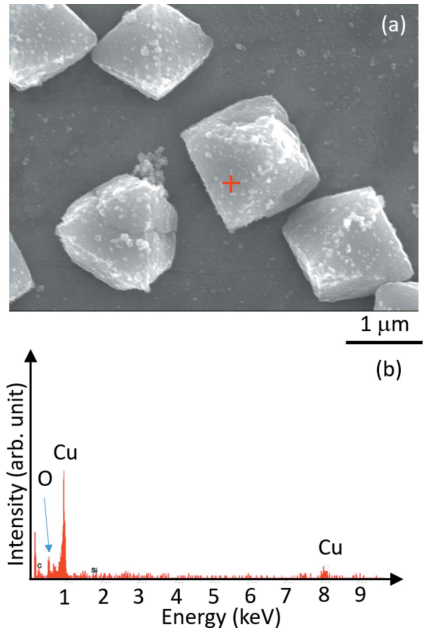

Figure 7
(*a*) SEM image and (*b*) EDX spectrum of particles synthesized and deposited on an Ni substrate.

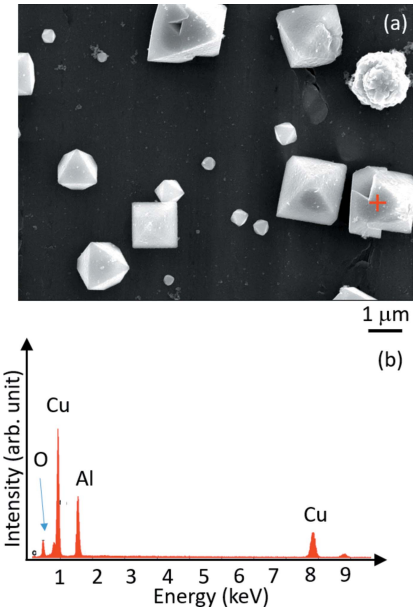

Figure 8
(*a*) SEM image and (*b*) EDX spectrum of particles synthesized and deposited on an Al substrate.

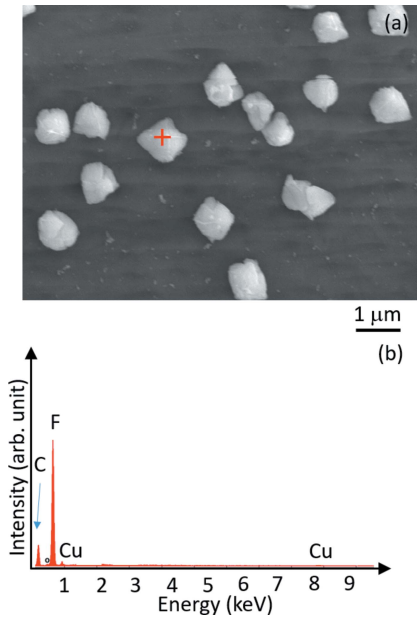

Figure 10
(*a*) SEM image and (*b*) EDX spectrum of particles synthesized and deposited on a PTFE substrate.

nated from CuO. The Raman signal at about 215 cm^{-1} and broad Raman peak structure ranging from 500 to 630 cm^{-1} originate from Cu_2O. By comparison with these Raman spectra, in the particles synthesized on Cu, Ni, $LiNbO_3$ and PTFE substrates, Cu_2O is included. The particles synthesized on Ni and $LiNbO_3$ substrates consist of both CuO and Cu_2O, while the particles synthesized on Cu substrate are made from the complex of Cu_2O and Cu_4O_3. These results may be reasonable for Cu/O (at %) ratios of the particles comparing with EDX analyses. Here, it allows us to deduce that the synthesized particle composition is strongly dependent on substrate type. Basically, the main component of the particles synthesized on a substrate except the Cu substrate tends to be CuO and Cu_2O. Consequently, cupric oxide particles consisting of mainly Cu_4O_3 are synthesized, grown and immobilized only on the Cu substrate, while the other conditions synthesized cupric particles composed mainly of CuO or Cu_2O. The results indicate that the composition of the synthesized and immobilized cupric particles is strongly dependent on substrate type.

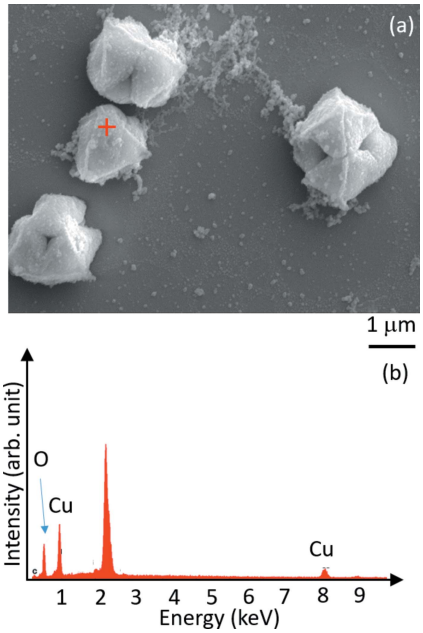

Figure 9
(*a*) SEM image and (*b*) EDX spectrum of particles synthesized and deposited on a 128° Y-cut $LiNbO_3$ substrate.

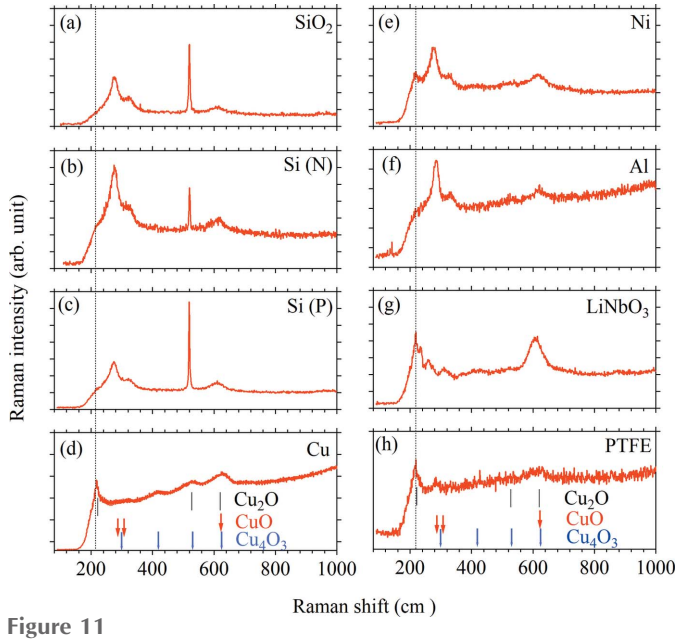

Figure 11
Micro-laser Raman spectra of particles immobilized on (*a*) SiO_2/Si, (*b*) n-doped Si, (*c*) p-doped Si, (*d*) Cu, (*e*) Ni, (*f*) Al, (*g*) 128° Y-cut $LiNbO_3$ and (*h*) PTFE substrates.

Here, paramelaconite, Cu_4O_3, is difficult to synthesize using normal methods. Cu_4O_3 is a naturally occurring scarce mineral (Zoolfakar *et al.*, 2014; Meyer *et al.*, 2012). Recently, some processes have succeeded in the synthesis of Cu_4O_3 that contains both +1 and +2 valence states with average composition $Cu_2^{+1}Cu_2^{+2}O_3$ as Wang *et al.* investigated the electronic structure (Wang *et al.*, 1996). Basically, it had only been synthesized as thin films, never as a bulk material. As described above, Wang *et al.* synthesized candy-like Cu_4O_3 particles successfully by microwave-irradiation synthesis method (Wang *et al.*, 2018). This photochemical reaction can provide bulk material of paramelaconite and immobilize it onto desired areas.

To date, many different approaches for the synthesis of nano/microstructured copper oxide have been investigated and implemented using not only vapor- but also liquid-phase-based methods. For example, physical vapor deposition including sputtering, thermal evaporation, thermal oxidation, molecular beam epitaxy, pulse vapor deposition and electron beam epitaxy have been used for the deposition of thin film and nanostructured copper oxide. Several groups have successfully demonstrated the synthesis of single CuO, Cu_2O and Cu_4O_3 phases by varying the oxygen flow rate using a reactive magnetron sputtering technique from a Cu target. Cu_4O_3 films have also been synthesized with a CuO target at a lower sputtering power (Zoolfakar *et al.*, 2014; Meyer *et al.*, 2012; Medina-Valtierra *et al.*, 2009).

Chemical vapor deposition processes, which are very popular deposition techniques, have often been used for depositing different Cu_xO stoichiometries. Medina-Valtierra *et al.* have demonstrated the synthesis of nanostructured Cu_4O_3 and CuO thin films (Medina-Valtierra *et al.*, 2009). Pola-Albores *et al.* have successfully demonstrated the deposition of Cu_4O_3 films on ZnO nano-rods using spray pyrolysis techniques (Pola-Albores *et al.*, 2012). The solid reaction between CuO and Cu_2O results in paramelaconite phase formation which can be described by (Zoolfakar *et al.*, 2014; Meyer *et al.*, 2012)

$$2CuO + Cu_2O \rightarrow Cu_4O_3. \quad (1)$$

Liquid-phase techniques including electrodeposition, hydrothermal/solvothermal and sol-gel are generally chosen due to their low cost and better control of the material's morphology at relatively low temperatures. Zhao *et al.* have synthesized pure polycrystalline Cu_4O_3 microspheres using copper (II) nitrate as the precursor in the presence of *N*,*N*-dimethylformamide and ethanol. They successfully deposited Cu_4O_3 films using the reaction of equation (1) in a closed system (Zhao *et al.*, 2012). In terms of the electrochemical reaction characteristics, as the lithium-ion storage electrodes deposited CuO thin film to enlarge the storage properties, the Cu_4O_3 phase appears. It is found that Cu_4O_3 plays an important role in the reversible electrochemical reactions that take place during the charging process (Chen *et al.*, 2015). Recently, Wang *et al.* have successfully synthesized Cu_4O_3 particles for the first time using a facile wet chemical method and investigated the formation mechanism based on a series of control experiments (Wang *et al.*, 2018). They reported that the candy-like Cu_4O_3 microstructure was formed via $Cu(NH_3)_4^{2+} \rightarrow Cu(OH)_4^{2-} \rightarrow Cu(OH)_2 \rightarrow CuO \rightarrow Cu_4O_3$ nuclei $\rightarrow Cu_4O_3$ crystal growth $\rightarrow$ candy-like Cu_4O_3. They also reported that the synthesized candy-like Cu_4O_3 microstructure exhibits good long-term antibacterial activities to both *E. coli* and *S. aureus* bacteria because the release of Cu^{2+} ions from the Cu_4O_3 is responsible for the antibacterial activity. On the other hand, Yamaguchi *et al.* have added the X-ray-radiolysis-induced photochemical synthesis of copper oxide materials as liquid-based phase reaction (Yamaguchi *et al.*, 2016*a*,*b*, 2017, 2019; Saegusa *et al.*, 2019). Until now, a single Cu_4O_3 phase has not been obtained by X-ray-irradiation of the liquid phase. In this study, the Cu_4O_3 phase is firstly synthesized by the X-ray-radiolysis-induced photochemical reaction.

On the surface of the Cu substrate, the Cu ions are always supplied to the spurs at which the X-ray-radiolysis-induced and secondary-electron-scattering-induced photochemical reaction occurs, as schematically illustrated in Figs. 1(*a*) and 1(*b*), respectively. The number of Cu ions is high enough to react near the Cu substrate. Therefore, the oxidization of Cu on Cu substrate is expected to proceed more slowly than the other cases, resulting in the Cu_4O_3 being synthesized, grown and deposited on the Cu substrate.

Two growth processes – habit formation and branching growth – govern the basic crystal shape. In habit formation, the relative order of surface energies of different crystallographic planes of a crystal determines the crystal habit. As a result, lower energy surfaces tend to increase in area, while higher energy surfaces are eliminated or reduced. Therefore, a habit can be modified when the relative order of the surface energies is altered or when crystal growth along certain directions is selectively hindered. In contrast, diffusion effects play a significant role in branching growth. Ions or molecules near the surface are consumed by the growth of the crystal. Then, a polyhedral crystal grows and the shape is dependent on the ion special distribution and kinetic coefficient in these regions. The crystal is grown to compensate for the diffusion effect resulting in faceting growth (Siegfried & Choi, 2005).

The results suggest that the substrate surface crystal structure and electronic state are sufficient to induce lateral distortion of growing crystal structures, with the type of structure formed depending primarily on the lattice constant of the terminated surface. The results suggest that Si(100) and Al substrates are good templates for the growth of ordered copper oxide particles. The surface morphology of copper oxide particles synthesized by the X-ray-radiolysis-induced photochemical reaction varies with substrate types dipped in the $Cu(COOCH_3)_2$ solution with the additive methanol.

4. Conclusion

We investigated the substrate type dependence of cupric particles synthesized by X-ray-radiolysis-induced photochemical reaction in $Cu(COOCH_3)_2$ liquid solution with the additive methanol. Comparing the morphologies of particles synthesized and immobilized on various types of substrates,

we found that the morphologies are strongly dependent on the substrate type. In addition, the substrate type also influences the particle composition.

Knowledge of the substrate type dependence of particle synthesis by X-ray-radiolysis-induced-photochemical reaction can provide flexibility within the constraints of any particular applications needs. This finding is essential for the exploration of nanostructures consisting of various copper metallic and oxide nanoparticles. This study opens the door to more innovative and novel routes to improve the future of the complex nanostructures and its many applications.

As Wang *et al.* demonstrated, the copper oxide microstructure exhibited useful antibacterial activity (Wang *et al.*, 2018). In addition, other copper oxides have been used for sensor devices (Tamaki *et al.*, 1998; Zaman *et al.*, 2011, 2012). Thus, as with the other copper oxide nanostructures, from this study emerges many potentials to develop three-dimensional printing or additive manufacturing processes for any of these applications (Sachs *et al.*, 1992; Gibson *et al.*, 2015; Saile *et al.*, 2009). The authors believe that this study of fabricating nanostructured Cu_4O_3 might provide possible novel materials insights and unique opportunities for incorporation into a wide range of applications.

Acknowledgements

We are grateful to Dr Atsushi Yamaguchi of Hyogo Prefectural Institute of Technology for SEM and EDX measurement support. We appreciate Dr Saiki and Dr Takizawa of Hyogo Prefectural Institute of Technology for fruitful discussions. We thank the Mitsutoyo Association for Science and Technology. This research and development work was supported in part by a JSPS Grants-in-Aid for Scientific Research B (No. 17H02755). These experiments were conducted at the BL8S2 of Aichi Synchrotron Radiation Center, Aichi Science and Technology Foundation, Aichi, Japan. (Proposal No. 2018a0016 and No. 2017a0049) with the financial support of Synchrotron Radiation Research Center, Nagoya University.

References

Akamatsu, K., Ikeda, S., Nawafune, H. & Yanagimoto, H. (2004). *J. Am. Chem. Soc.* **126**, 10822–10823.
Bae, C. H., Nam, S. H. & Park, S. M. (2002). *Appl. Surf. Sci.* **197–198**, 628–634.
Bárta, J., Pospíšil, M. & Čuba, V. (2010). *J. Radioanal. Nucl. Chem.* **286**, 611–618.
Bharti, A., Bhardwaj, R., Agrawal, N., Goyal, S. & Gautam, S. (2016). *Sci. Rep.* **6**, 22394.
Borse, P. H., Yi, J. M., Je, J. H., Tsai, W. L. & Hwu, Y. (2004). *J. Appl. Phys.* **95**, 1166–1170.
Chen, W., Zhang, H., Ma, Z., Yang, B. & Li, Z. (2015). *J. Mater. Chem. A*, **3**, 14202–14209.
Debbichi, L., Marco de Lucas, M. C., Pierson, J. F. & Krüger, P. (2012). *J. Phys. Chem. C*, **116**, 10232–10237.
Dey, G. R. (2005). *Radiat. Phys. Chem.* **74**, 172–184.
Gibson, I., Rosen, D. & Stucker, B. (2015). *Additive Manufacturing Technologies – 3D Printing, Rapid Prototyping, and Direct Digital Manufaturing*, 2nd ed. Springer.
Izaki, M., Shinagawa, T., Mizuno, K., Ida, Y., Inaba, M. & Tasaka, A. (2007). *J. Phys. D Appl. Phys.* **40**, 3326–3329.
Jonah, C. D. & Miller, J. R. (1977). *J. Phys. Chem.* **81**, 1974–1976.
Karadas, F., Ertas, G., Ozkaraoglu, E. & Suzer, S. (2005). *Langmuir*, **21**, 437–442.
La Mer, V. K. (1952). *Ind. Eng. Chem.* **44**, 1270–1277.
La Mer, V. K. & Dinegar, R. H. (1950). *J. Am. Chem. Soc.* **72**, 4847–4854.
Ma, Q., Moldovan, N., Mancini, D. C. & Rosenberg, R. A. (2000). *Appl. Phys. Lett.* **76**, 2014–2016.
Medina-Valtierra, J., Frausto-Reyes, C., Camarillo-Martínez, G. & Ramírez-Ortiz, J. A. (2009). *Appl. Catal. Gen.* **356**, 36–42.
Meyer, B. K., Polity, A., Reppin, D., Becker, M., Hering, P., Klar, P. J., Sander, Th., Reindl, C., Benz, J., Eickhoff, M., Heiliger, C., Heinemann, M., Bläsing, J., Krost, A., Shokovets, S., Müller, C. & Ronning, C. (2012). *Phys. Status Solidi B*, **249**, 1487–1509.
Oyanagi, H., Orimoto, Y., Hayakawa, K., Hatada, K., Sun, Z., Zhang, L., Yamashita, K., Nakamura, H., Uehara, M., Fukano, A. & Maeda, H. (2014). *Sci. Rep.* **4**, 7199.
Poizot, P., Laruelle, S., Grugeon, S., Dupont, L. & Tarascon, J. M. (2000). *Nature*, **407**, 496–499.
Pola-Albores, F., Antúnez-Flores, W., Amézaga-Madrid, P., Ríos-Valdovinos, E., Valenzuela-Zapata, M., Paraguay-Delgado, F. & Miki-Yoshida, M. (2012). *J. Cryst. Growth*, **351**, 77–82.
Remita, S., Fontaine, P., Lacaze, E., Borensztein, Y., Sellame, H., Farha, R., Rochas, C. & Goldmann, M. (2007). *Nucl. Instrum. Methods Phys. Res. B*, **263**, 436–440.
Sachs, E., Cima, M., Williams, P., Brancazio, D. & Cornie, J. (1992). *J. Eng. Ind.* **114**, 481–488.
Saegusa, S., Sakurai, I., Okada, I., Fukuoka, T., Suzuki, S., Utsumi, Y. & Yamaguchi, A. (2019). *Trans. Jpn Inst. Electronics Packaging*, **12**, E19-003.
Saile, V., Wallradbe, U., Tabata, O. & Korvink, J. G. (2009). *Advanced Micro and Nanosystems*, Vol. 7, *LIGA and its Applications.* Weinheim: Wiley-VCH.
Siegfried, M. J. & Choi, K. (2005). *Angew. Chem. Int. Ed.* **44**, 3218–3223.
Su, D., Xie, X., Dou, S. & Wang, G. (2015). *Sci. Rep.* **4**, 5753.
Tamaki, J., Shimanoe, K., Yamada, Y., Yamamoto, Y., Miura, N. & Yamazoe, N. (1998). *Sens. Actuators B Chem.* **49**, 121–125.
Volanti, D. P., Keyson, D., Cavalcante, L. S., Simões, A. Z., Joya, M. R., Longo, E., Varela, J. A., Pizani, P. S. & Souza, A. G. (2008). *J. Alloys Compd.* **459**, 537–542.
Wang, L., Wu, H., Desai, S. R. & Lou, L. (1996). *Phys. Rev. B*, **53**, 8028–8031.
Wang, W., Zhu, L., Lv, P., Liu, G., Yu, Y. & Li, J. (2018). *Appl. Mater. Interfaces*, **10**, 37287–37297.
Yamaguchi, A., Fukuoka, T., Okada, I., Ishihara, M., Sakurai, I. & Utsumi, Y. (2017). *J. Synchrotron Rad.* **24**, 653–660.
Yamaguchi, A., Matsumoto, T., Okada, I., Sakurai, I. & Utsumi, Y. (2015). *Mater. Chem. Phys.* **160**, 205–211.
Yamaguchi, A., Okada, I., Fukuoka, T., Ishihara, M., Sakurai, I. & Utsumi, Y. (2016*b*). *J. Nanomater.* **2016**, 8584304.
Yamaguchi, A., Okada, I., Fukuoka, T., Sakurai, I. & Utsumi, Y. (2016*a*). *Jpn. J. Appl. Phys.* **55**, 055502.
Yamaguchi, A., Okada, I., Sakurai, I., Izumi, H., Ishihara, M., Fukuoka, T., Suzuki, S., Elphick, K., Jackson, E., Hirohata, A. & Utsumi, Y. (2019). *J. Synchrotron Rad.* **26**, 1986–1995.
Yamaguchi, H., Uchihori, Y., Yasuda, N., Takada, M. & Kitamura, H. (2005). *J. Radiat. Res. (Tokyo)*, **46**, 333–341.
Zaman, S., Asif, M. H., Zainelabdin, A., Amin, G., Nur, O. & Willander, M. (2011). *J. Electroanal. Chem.* **662**, 421–425.
Zaman, S., Zainelabdin, A., Amin, G., Nur, O. & Willander, M. (2012). *J. Phys. Chem. Solids*, **73**, 1320–1325.
Zhang, Q., Zhang, K., Xu, D., Yang, G., Huang, H., Nie, F., Liu, C. & Yang, S. (2014). *Prog. Mater. Sci.* **60**, 208–337.
Zhao, L., Chen, H., Wang, Y., Che, H., Gunawan, P., Zhong, Z., Li, H. & Su, F. (2012). *Chem. Mater.* **24**, 1136–1142.
Zoolfakar, A. S., Rani, R. A., Morfa, A. J., O'Mullane, A. P. & Kalantar-zadeh, K. (2014). *J. Mater. Chem. C*, **2**, 5247–5270.